Article

Molecular Cell

mTORC1-Regulated and HUWE1-Mediated WIPI2 Degradation Controls Autophagy Flux

Graphical Abstract

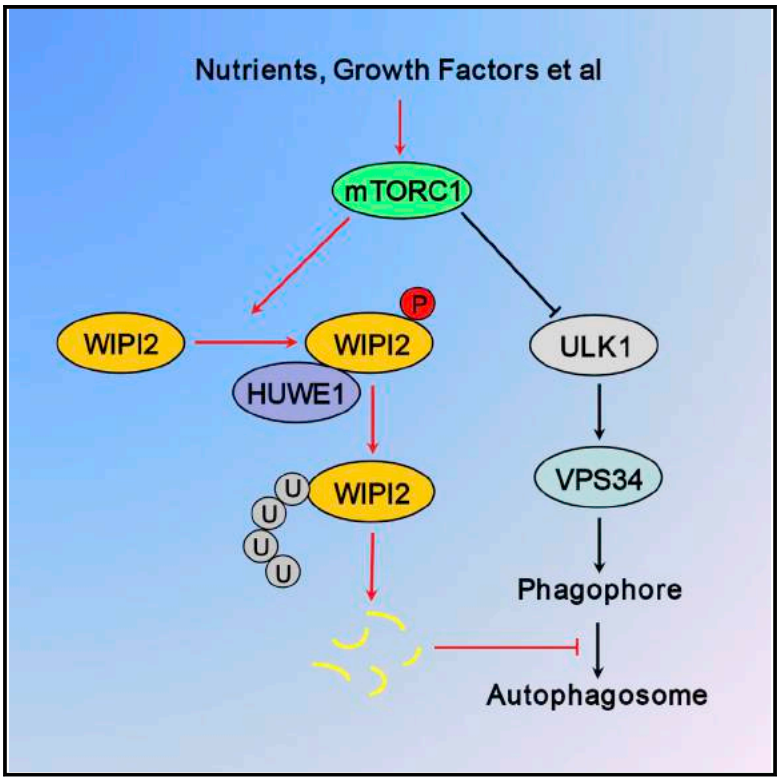

Authors

Wei Wan, Zhiyuan You, Li Zhou, ..., Cong Yi, Yin Shi, Wei Liu

Correspondence

liuwei666@zju.edu.cn

In Brief

Wan et al. report a direct involvement of mTORC1 in the control of phagophore growth. mTORC1-dependent phosphorylation directs WIPI2 to interact with its E3 ubiquitin ligase HUWE1, which leads to WIPI2 degradation and autophagy inhibition. This WIPI2 quantity control pathway is a key determinant of constitutive and adaptive autophagy.

Highlights

- HUWE1 mediates the ubiquitination and degradation of WIPI2
- mTORC1 promotes WIPI2 degradation by phosphorylating WIPI2
- Phosphorylation at Ser395 of WIPI2 enhances HUWE1 interaction
- WIPI2 level determines autophagy flux and lipid clearance

Wan et al., 2018, Molecular Cell 72, 303–315
October 18, 2018
https://doi.org/10.1016/j.molcel.2018.09.017

CellPress

Molecular Cell
Article

mTORC1-Regulated and HUWE1-Mediated WIPI2 Degradation Controls Autophagy Flux

Wei Wan,[1] Zhiyuan You,[1] Li Zhou,[1] Yinfeng Xu,[1] Chao Peng,[3] Tianhua Zhou,[1] Cong Yi,[1] Yin Shi,[1] and Wei Liu[1,2,4,*]
[1]Department of Biochemistry and Department of Cardiology of the Second Affiliated Hospital, Zhejiang University School of Medicine, Hangzhou 310058, China
[2]Collaborative Innovation Center for Diagnosis and Treatment of Infectious Disease, First Affiliated Hospital, Zhejiang University School of Medicine, Hangzhou 310003, China
[3]National Center for Protein Science Shanghai, Institute of Biochemistry and Cell Biology, Shanghai Institutes of Biological Sciences, Chinese Academy of Sciences, Shanghai 200031, China
[4]Lead Contact
*Correspondence: liuwei666@zju.edu.cn
https://doi.org/10.1016/j.molcel.2018.09.017

SUMMARY

mTORC1, the major homeostatic sensor and responder, regulates cell catabolism mainly by targeting autophagy. Here, we show that mTORC1 directly controls autophagosome formation via phosphorylation of WIPI2, a critical protein in isolation membrane growth and elongation. mTORC1 phosphorylates Ser395 of WIPI2, directing WIPI2 to interact specifically with the E3 ubiquitin ligase HUWE1 for ubiquitination and proteasomal degradation. Physiological or pharmacological inhibition of mTORC1 in cells promotes WIPI2 stabilization, autophagosome formation, and autophagic degradation. In mouse liver, fasting significantly increases the WIPI2 protein level, while silencing HUWE1 enhances autophagy, and introducing WIPI2 improves lipid clearance. Thus, regulation of the intracellular WIPI2 protein level by mTORC1 and HUWE1 is a key determinant of autophagy flux and may coordinate the initiation, progression, and completion of autophagy.

INTRODUCTION

Autophagy is a highly conserved self-digestion pathway in which intracellular materials are engulfed by double-membrane structures and delivered to lysosomes for degradation (Lamb et al., 2013). While basal autophagy is required for cells to maintain homeostasis through elimination of protein aggregates and damaged organelles, autophagy is significantly activated under stress conditions to reprogram cell metabolism (Levine and Kroemer, 2008; Mizushima et al., 2008). As a multistage process, autophagy comprises initiation, membrane nucleation, membrane growth and extension, autophagosome maturation, and lysosomal degradation, with distinct sets of proteins governing the different phases (Yu et al., 2018). Genetic studies from yeast to mammals have established a hierarchy of recruitment, hetero-assembly, and activation of autophagy-related proteins (Atgs) in the pathway (Itakura and Mizushima, 2010; Suzuki et al., 2007).

Mammalian target of rapamycin complex 1 (mTORC1), the master regulator of cell growth and cell metabolism, has emerged as a regulator of autophagy at several stages. In response to intracellular and extracellular cues, mTORC1 activity is directly linked to autophagy initiation (Dunlop and Tee, 2014; Yang and Klionsky, 2010). It suppresses the synthesis of the autophagic pool of phosphatidylinositol 3-phosphate (PI3P), required for membrane nucleation, by phosphorylating both Unc51-like kinase 1 (ULK1) and Atg13, two components of the ULK1 complex, and Atg14L, an essential subunit of the class III phosphoinositide 3-kinase VPS34 complex (Chang and Neufeld, 2009; Ganley et al., 2009; Hosokawa et al., 2009; Jung et al., 2009; Kim et al., 2011; Yuan et al., 2013). Furthermore, mTORC1 inhibits autophagosome maturation and activates autolysosomal tubulation by phosphorylating UVRAG (Kim et al., 2015; Munson et al., 2015). Moreover, mTORC1 takes control of lysosomal activity by regulating TFEB, the major transcription factor for lysosome biogenesis (Roczniak-Ferguson et al., 2012; Settembre et al., 2011, 2012). Recently, it has also been suggested that mTORC1 directly phosphorylates and activates the histone acetyltransferase p300, leading to the inactivation of Atg proteins, including LC3, Atg5, and Atg7, which are required for the biogenesis of autophagosomes (Huang et al., 2015; Lee and Finkel, 2009; Wan et al., 2017).

Formation of the phagophore from the endoplasmic reticulum (ER) membranes relies on the local synthesis and enrichment of PI3P by the VPS34 complex (Backer, 2008; Simonsen and Tooze, 2009; Wirth et al., 2013). After that, a key event for phagophore expansion is the recruitment of WIPI2 (a mammalian ortholog of yeast Atg18), a WD40-repeat-containing PI3P-binding protein. WIPI2 then facilitates LC3 lipidation and the subsequent growth of the phagophore by recruiting the Atg12-Atg5-Atg16L1 complex (Dooley et al., 2014; Polson et al., 2010). In addition, it has recently been suggested that WIPI2 tethers the phagophore with the ER (Zhao et al., 2017) and can be recruited by TBK1 to cytosol-invading bacteria for anti-bacterial autophagy (Thurston et al., 2016). All these mechanisms highlight a pivotal role of WIPI2 in autophagosome formation. The expression of WIPI2 is known to be controlled by TFEB (Settembre et al., 2011) and ZKSCAN3, a zinc-finger family DNA-binding protein (Chauhan et al., 2013). Furthermore, multiple components of the autophagy machinery are known to undergo post-translational modification

and/or ubiquitination-mediated proteasomal degradation (Lee et al., 2008; Liu et al., 2016; Platta et al., 2012; Wei et al., 2013; Yang et al., 2013; Zhang et al., 2015). Nevertheless, we know very little about the mechanisms controlling the quality and quantity of WIPI2 protein.

In this study, we have identified WIPI2 as a novel substrate of mTORC1 and a target of the E3 ubiquitin ligase HUWE1. By revealing the strong link between mTORC1-mediated phosphorylation and HUWE1-dependent ubiquitination and degradation of WIPI2, we prove that this WIPI2-based regulatory mechanism is essential for the control of autophagy flux *in vitro* and *in vivo*.

RESULTS

HUWE1 Mediates WIPI2 Ubiquitination and Degradation

To identify new interaction partners of WIPI2, we screened them in HEK293T cells stably expressing WIPI2-myc using mass spectrometry (Table S1). The proteins pulled down by WIPI2-myc included known WIPI2-binding proteins, such as Atg16L1 (Dooley et al., 2014). Proteins related to the ubiquitin-proteasome system were also highly abundant (Table S1). Among them, the E3 ubiquitin ligase HUWE1 has previously been shown to have an affinity with WIPI2 by affinity proteomics using HUWE1 as bait (Thompson et al., 2014). To verify the potential interaction between WIPI2 and HUWE1, we carried out co-immunoprecipitation assays in mouse embryonic fibroblasts (MEFs). As expected, immunoprecipitation of WIPI2 co-precipitated HUWE1 and Atg16L1, but not Atg7 (Figure 1A). Intriguingly, HUWE1 was not co-precipitated with WIPI1, another member of the WIPI family (Figure 1B), indicating a specific association between WIPI2 and HUWE1. Also, purified recombinant glutathione S-transferase (GST)-WIPI2 pulled down endogenous HUWE1 from the cell lysates (Figure 1C).

We then analyzed the potential effect of the interaction on WIPI2. When silencing HUWE1 in cells increased the WIPI2 protein level (Figures 1D and 1E), overexpressing HUWE1 decreased WIPI2 in a dose-dependent manner (Figures 1F and 1G), while neither of them changed the mRNA level of *WIPI2* (Figure S1A). In addition, treating cells with the proteasome inhibitor MG132, but not the lysosome inhibitor chloroquine (CQ), raised intracellular WIPI2 and restored WIPI2 in HUWE1-overexpressing cells (Figures 1H and 1I), suggesting that WIPI2 turnover depends on the ubiquitin-proteasome system. Consistent with this, HUWE1 silencing reduced WIPI2 ubiquitination, while HUWE1 overexpression enhanced it (Figures 1J, 1K, and S1B). Furthermore, *in vitro* ubiquitination assays indicated that, in the presence of purified ubiquitin, E1, E2, and HUWE1, purified recombinant WIPI2 underwent dramatic ubiquitination, which was not seen when E1, E2, or ubiquitin was absent or when inactive E2 or HUWE1 was used (Figure 1L). To identify the ubiquitination site(s) of WIPI2, we analyzed the ubiquitinated WIPI2 from the *in vitro* ubiquitination assay with mass spectrometry. Five lysine residues (K128, K198, K205, K219, and K265) were suggested (Figure S2A). A WIPI2 mutant was then constructed in which all the five lysine residues were replaced by arginine (WIPI2-5KR). In transfected cells, compared to wild-type (WT) WIPI2, WIPI2-5KR demonstrated much lower basal ubiquitination (Figure S2B). The expression and ubiquitination of WIPI2-5KR showed no response to HUWE1 overexpression (Figures S2B and S2C). Together, these results suggest that WIPI2 is a direct ubiquitination substrate of HUWE1, which mediates its proteasomal degradation.

WIPI2 Is Upregulated during Autophagy

We sought to determine whether HUWE1-mediated WIPI2 degradation responds to autophagic stimuli, because of the essential role of WIPI2 in autophagy. Strikingly, intracellular WIPI2 protein increased greatly in cells treated with starvation or mTORC1 inhibitor, two classical autophagy inducers, while other components of the autophagic machinery and HUWE1 were unchanged (Figures 2A and 2B). As *WIPI2* is a target gene of TFEB, whose activity is negatively regulated by mTORC1 (Roczniak-Ferguson et al., 2012; Settembre et al., 2012), we treated cells with Torin1 for a short time (3 hr) and a long time (24 hr). We found that the *WIPI2* mRNA level was notably upregulated only under long-term Torin1 treatment (Figure S3A), suggesting that the observed increase in WIPI2 protein was due to reduced degradation. We also examined whether autophagic signaling affects human WIPI2, which has several isoforms compared to the single one in mouse. We found that, among the four tested human WIPI2 isoforms, WIPI2a and WIPI2b protein levels were increased by cell starvation (Figure S3B). Furthermore, in HUWE1-depleted or MG132-treated MEFs, cell starvation or Torin1 treatment could not further elevate the WIPI2 protein level (Figures 2C–2F).

We thus investigated the interaction between WIPI2 and HUWE1. Co-immunoprecipitation detected the binding of endogenous WIPI2 with transfected His-HUWE1, which was dramatically reduced by cell starvation or Torin1 treatment (Figures 2G and 2H). Accordingly, WIPI2 ubiquitination was greatly decreased under the same conditions (Figures 2I and S3C). In addition, the turnover of cellular WIPI2 in cycloheximide (CHX)-treated MEFs was inhibited by knockdown of HUWE1 or treatment with Torin1 (Figures 2J–2M). Together, these data suggest that WIPI2 is upregulated during autophagy by a reduction in HUWE1-mediated degradation.

mTORC1 Phosphorylates WIPI2 at Ser395

Raptor and mLST8, two essential subunits of mTORC1, are among the potential interacting partners of WIPI2 in our screen (Table S1). This prompted us to explore a potential association between mTORC1 and WIPI2. We examined in cells the interaction of WIPI2 and Raptor, which recognizes and interacts with mTORC1 substrates (Nojima et al., 2003; Yu et al., 2011). Co-immunoprecipitation detected an association of Myc-tagged WIPI2, but not WIPI1, with endogenous Raptor (Figure 3A). In response to abundant amino acids, mTORC1 is targeted to the lysosomal surface by the Rag-Ragulator complex, where it is activated and interacts with its substrates in many cases (Martina and Puertollano, 2013; Sancak et al., 2010; Settembre et al., 2012; Wan et al., 2017). In addition, WIPI2 is detectable on autophagosomes (Polson et al., 2010), suggesting the possibility that WIPI2 may target to lysosomes when autophagosomes fuse with lysosomes. To check whether WIPI2 resides on lysosomes, we performed a lysosome precipitation assay in $Atg5^{+/+}$ and $Atg5^{-/-}$ MEFs. Cells expressing GFP-tagged

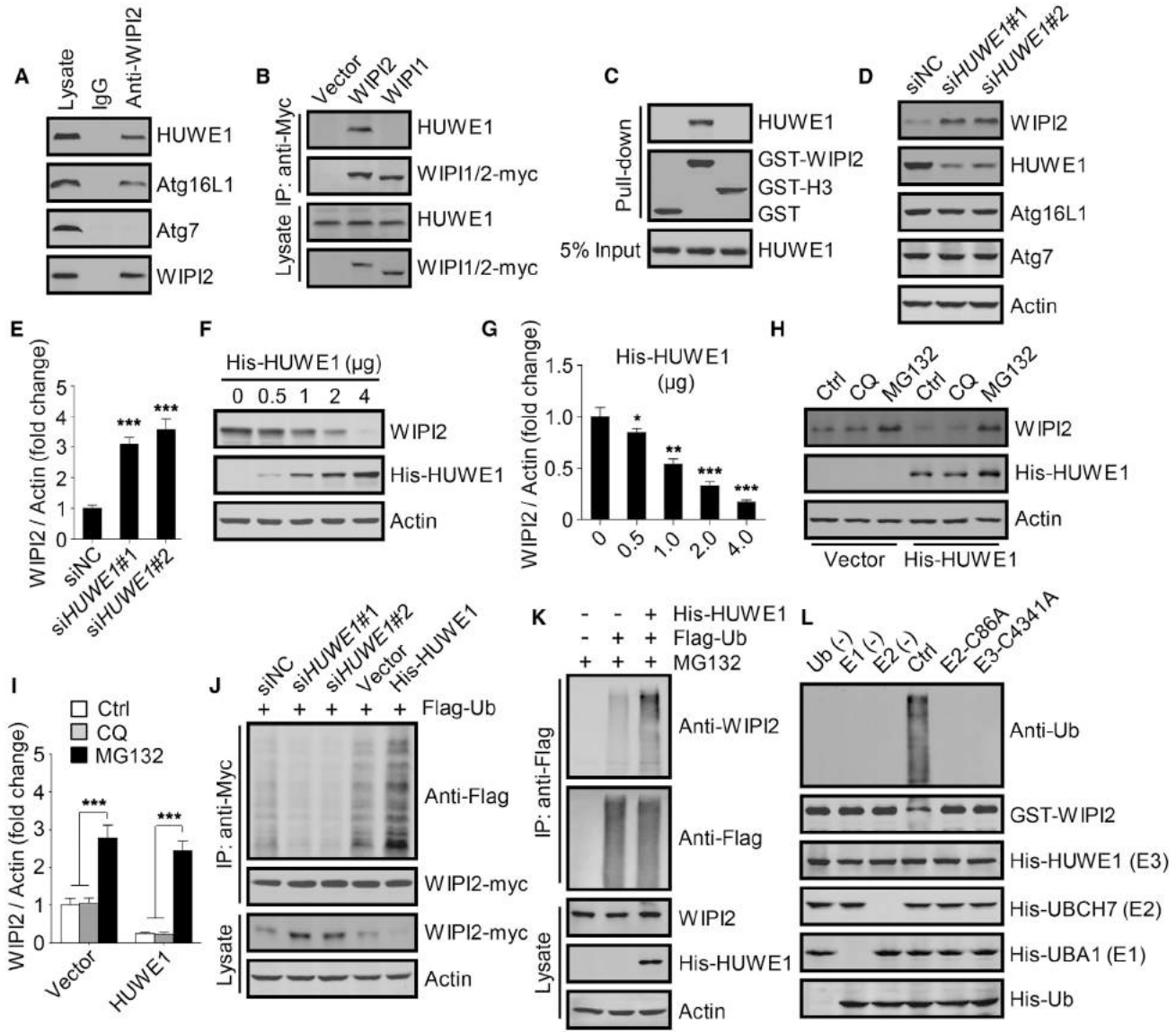

Figure 1. HUWE1 Mediates WIPI2 Ubiquitination and Degradation

(A) Co-immunoprecipitation of HUWE1 with WIPI2 in MEFs. Endogenous WIPI2 was immunoprecipitated using anti-WIPI2, and the immunoprecipitates were analyzed with anti-HUWE1, anti-Atg16L1, or anti-Atg7. IgG, immunoglobulin G.

(B) Co-immunoprecipitation of endogenous HUWE1 with exogenous WIPI2 or WIPI1 in HEK293T cells. Myc-tagged WIPI2 or WIPI1 was immunoprecipitated using anti-Myc.

(C) Purified recombinant GST-WIPI2 or GST-histone H3 was incubated with MEF lysates, and the bound HUWE1 was detected by western blot.

(D–I) Western blot analysis of WIPI2 levels in MEFs. The cells were incubated with small interfering RNAs (siRNAs) against HUWE1 (D and E), subjected to increasing levels of His-HUWE1 transfection (F and G), or treated by chloroquine (CQ) or MG132 with or without His-HUWE1 transfection (4.0 μg) (H and I). Western blots are shown in (D), (F), and (H), and quantifications are presented in (E), (G), and (I), respectively. The statistical data are presented as mean ± SEM of three independent experiments. *$p < 0.05$; **$p < 0.01$; ***$p < 0.001$.

(J) Ubiquitination of WIPI2-myc in HEK293T cells co-expressing Flag-ubiquitin. The cells were incubated with HUWE1 siRNAs or transfected with His-HUWE1. WIPI2-myc was immunoprecipitated using anti-Myc, and the immunoprecipitates were analyzed by anti-Flag.

(K) Ubiquitination of endogenous WIPI2 in MEFs expressing Flag-ubiquitin. The MEFs with or without His-HUWE1 transfection were treated with MG132 for 6 hr; then the cell lysates were subjected to anti-Flag immunoprecipitation, and the immunoprecipitates were analyzed by western blot using anti-WIPI2.

(L) *In vitro* ubiquitination assay of purified GST-WIPI2. The reactions were performed either with purified His-tagged ubiquitin, UBA1 (E1), UBCH7 (E2) or its inactive mutant (C86A), and HUWE1 or its inactive mutant (C4341A) or in the absence of UBA1, UBCH7, or ubiquitin.

See also Figures S1 and S2 and Table S1.

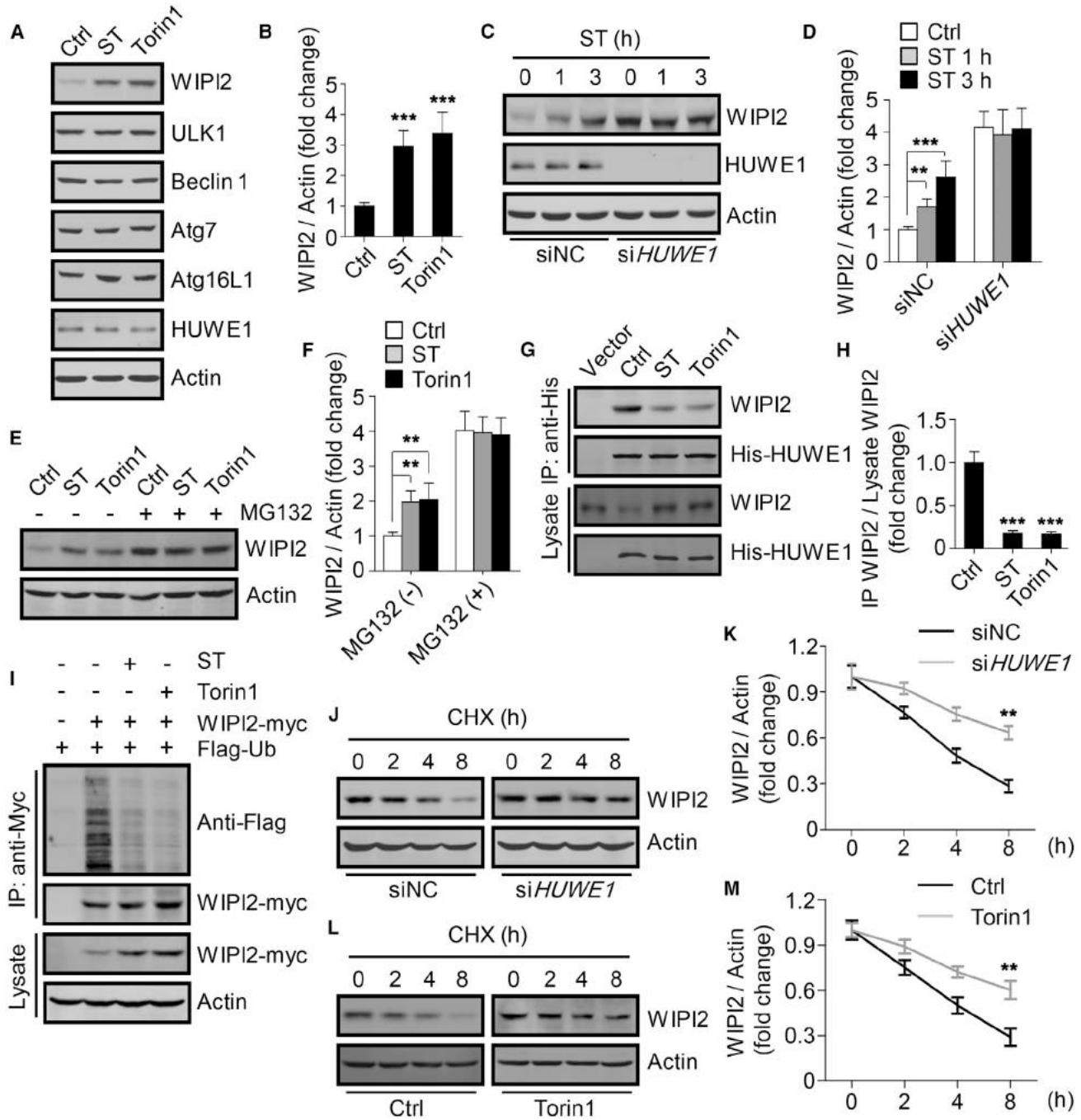

Figure 2. WIPI2 Is Upregulated during Autophagy

(A and B) Western blot analysis of the indicated autophagy-related proteins and HUWE1 in MEFs treated with starvation medium (ST) or Torin1 (A). Quantification is presented in (B).

(C–F) WIPI2 levels in starved MEFs with or without HUWE1 silencing (C and D) or in starved or Torin1-treated MEFs with or without MG132 (E and F). Western blots are presented in (C) and (E), and quantifications are presented in (D) and (F), respectively.

(G and H) Co-immunoprecipitation of endogenous WIPI2 with transfected His-HUWE1 in MEFs treated with starvation or Torin1 (G). His-HUWE1 was immunoprecipitated using anti-His, and the immunoprecipitates were analyzed using anti-WIPI2. Quantification is presented in (H).

(I) Ubiquitination of WIPI2-myc in HEK293T cells co-expressing Flag-ubiquitin treated as in (G). WIPI2-myc was immunoprecipitated using anti-Myc, and the immunoprecipitates were analyzed using anti-Flag.

(legend continued on next page)

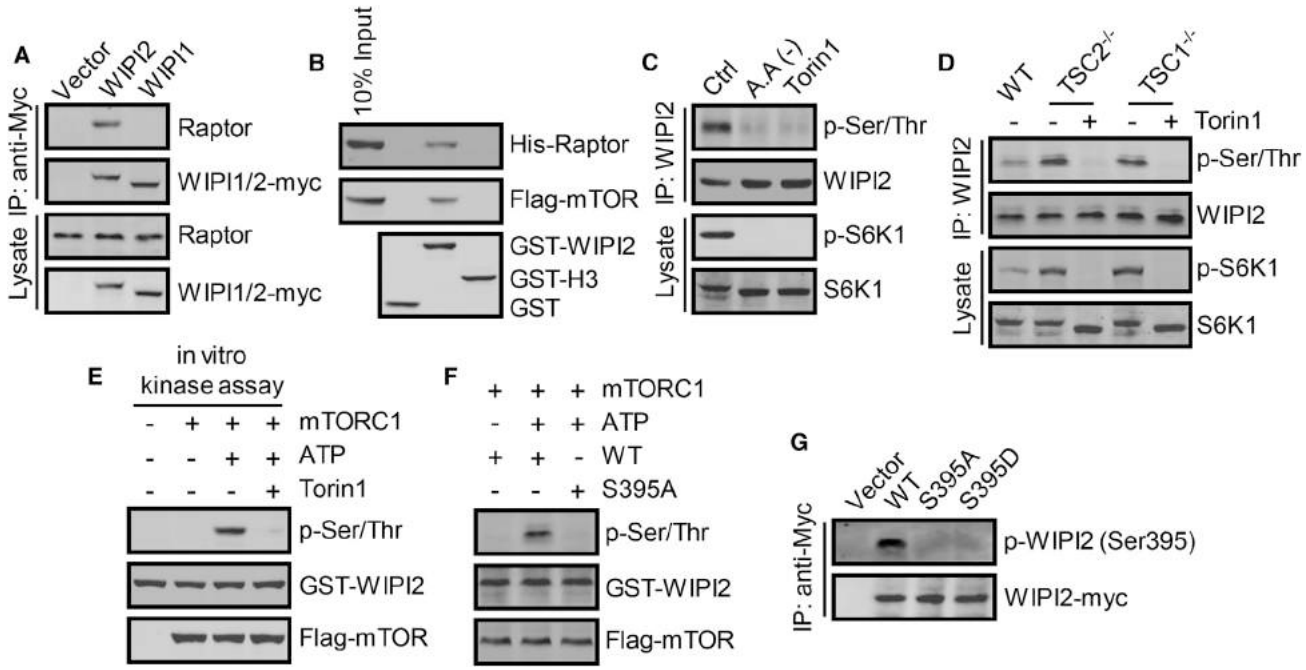

Figure 3. mTORC1 Phosphorylates WIPI2 at Ser395

(A) Co-immunoprecipitation of endogenous Raptor with transfected Myc-tagged WIPI2 or WIPI1 in HEK293T cells. WIPI2-myc or WIPI1-myc was immunoprecipitated using anti-Myc.

(B) Recombinant mTORC1 comprising Flag-mTOR, His-Raptor, and His-mLST8 was incubated with purified GST-WIPI2 or GST-histone H3. The GST-WIPI2 or GST-histone H3 was then pulled down using glutathione Sepharose beads, and the bound Flag-mTOR and His-Raptor were detected by western blot using anti-Flag and anti-His.

(C and D) Phosphorylation of WIPI2 in WT MEFs treated with amino-acid-free medium or Torin1 (C) or in TSC1$^{-/-}$ or TSC2$^{-/-}$ MEFs with or without Torin1 treatment (D). WIPI2 immunoprecipitated from cells were analyzed by western blot using anti-phospho-serine/threonine, and the cell lysates were analyzed using anti-S6K1 and anti-phospho-S6K1 (Thr389).

(E and F) *In vitro* kinase assay using recombinant mTORC1 and purified GST-WIPI2 or GST-WIPI2-S395A as a substrate. GST-WIPI2 or GST-WIPI2-S395A was pulled down using glutathione Sepharose beads and analyzed by western blot using anti-phospho-serine/threonine.

(G) Phosphorylation of Myc-tagged WIPI2 or WIPI2 mutants expressed in HEK293T cells. Myc-tagged WIPI2s were immunoprecipitated with anti-Myc and analyzed by western blot using a specific antibody against phospho-WIPI2 (Ser395).

See also Figure S4 and Table S1.

TMEM192, a lysosomal transmembrane protein (Abu-Remaileh et al., 2017), were homogenized without detergent, and lysosomes were pulled down with a specific GFP antibody. Following incubation with protein A agarose beads, lysosomes bound to the beads were analyzed by western blot. WIPI2 was clearly co-precipitated with lysosomes in MEFs with or without Atg5, but another cytoplasmic protein, tubulin, was not (Figure S4A). This suggests that WIPI2 is able to target lysosomes independent of autophagosomes. Next, we carried out an *in vitro* pull-down assay to identify a direct interaction between mTORC1 and WIPI2. Purified recombinant GST-WIPI2 was incubated with purified recombinant mTORC1 comprising mTOR, Raptor, and mLST8. When GST-WIPI2 was precipitated by glutathione Sepharose beads, mTOR and Raptor were also pulled down (Figure 3B). To test whether WIPI2 could be a phosphorylation substrate of mTORC1, we used a specific phospho-serine/threonine antibody to examine the phosphorylation status of WIPI2 immunoprecipitated from cells. Serine/threonine phosphorylation of WIPI2 was detected in fed control cells; however, this was strikingly suppressed when cellular mTORC1 activity was inhibited by treating the cells with amino-acid-free medium or Torin1 (Figure 3C). Accordingly, TSC1- or TSC2-deleted MEFs, in which mTORC1 was constitutively activated, displayed a much higher basal phosphorylation of WIPI2 than WT MEFs (Figure 3D). These data suggest that the phosphorylation of WIPI2 at serine/threonine residues is regulated by mTORC1. We then performed an *in vitro* kinase assay using recombinant full-length WIPI2 and recombinant mTORC1. Direct phosphorylation of WIPI2 by mTORC1 was revealed, and the level of the phosphorylation was high enough to detect with unlabeled

(J–M) WIPI2 levels in cycloheximide (CHX)-treated MEFs with or without HUWE1 RNAi (J and K) or Torin1 treatment (L and M). Western blots are presented in (J) and (L), and quantifications are presented in (K) and (M), respectively. CHX was added to culture medium 48 hr after HUWE1 RNAi, or with or without Torin1, for the indicated time.

All the statistical data are presented as mean ± SEM of three independent experiments. $^{**}p < 0.01$; $^{***}p < 0.001$.

See also Figure S3.

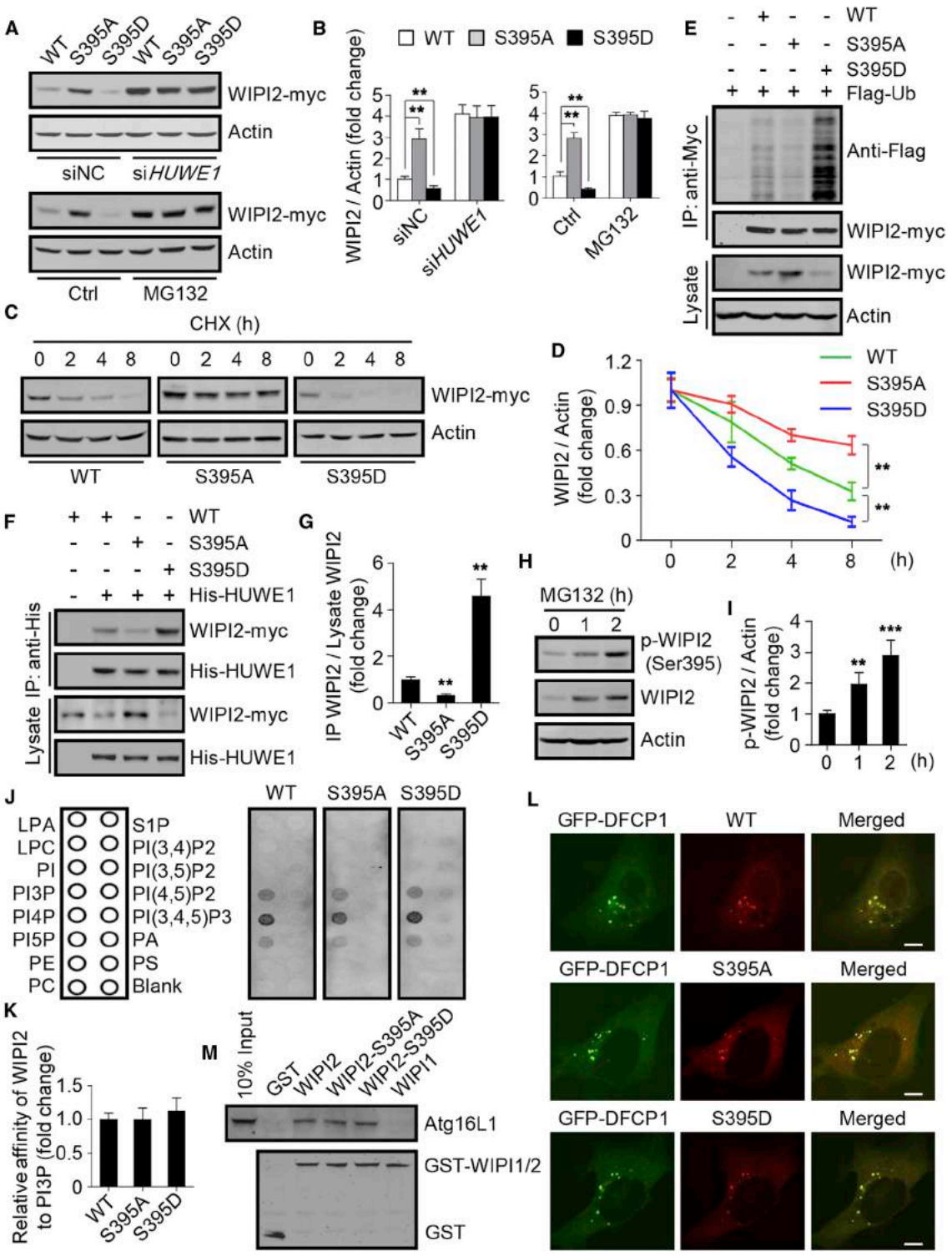

Figure 4. mTORC1-Mediated Phosphorylation Promotes WIPI2 Degradation

(A–D) WIPI2-myc levels in HEK293T cells stably expressing Myc-tagged WT WIPI2 or each of the WIPI2 mutants with HUWE1 RNAi or MG132 treatment (A and B), or CHX treatment (C and D). Western blots are presented in (A) and (C), and quantifications are presented in (B) and (D), respectively.

(E) WIPI2-myc ubiquitination in the stable cell lines with transient transfection of Flag-ubiquitin. The WIPI2s were immunoprecipitated using anti-Myc, and the immunoprecipitates were analyzed using anti-Flag.

(legend continued on next page)

ATP and an anti-phospho-serine/threonine antibody rather than ^{32}P-labeled ATP and autoradiography (Figure 3E).

To identify the mTORC1 phosphorylation site(s) on WIPI2, we analyzed the phosphorylated full-length WIPI2 from the *in vitro* kinase assay with mass spectrometry. Ser395, which fits perfectly with mTORC1 consensus motifs (Hsu et al., 2011) and is highly conserved among species, was suggested (Figures S4B and S4C). We then created a WIPI2 mutant by replacing Ser395 with alanine and performed *in vitro* kinase assays using purified recombinant mTORC1 and WIPI2 proteins. mTORC1 phosphorylated WT WIPI2 but not WIPI2-S395A (Figure 3F). Accordingly, using an antibody against WIPI2 specifically phosphorylated at Ser395, we found that phosphorylation was detectable in the immunoprecipitates of WT WIPI2, but not of WIPI2-S395A, or of WIPI2-S395D, in which Ser395 was replaced by aspartic acid (Figure 3G). Together, these results suggest that WIPI2 is a direct phosphorylation substrate of mTORC1 and that Ser395 is the major site of phosphorylation by mTORC1.

mTORC1-Mediated Phosphorylation Promotes WIPI2 Degradation

To examine the functional effect of mTORC1-mediated phosphorylation of WIPI2, we generated HEK293T cell lines stably expressing WT WIPI2 or the amino-acid substitution mutants WIPI2-S395A, which cannot be phosphorylated, and WIPI2-S395D, which mimics phosphorylated WIPI2. In these cell lines, the relative level of protein expression was WIPI2-S395A > WT WIPI2 > WIPI2-S395D (Figures 4A and 4B). Intriguingly, HUWE1 knockdown or MG132 treatment abolished the elevation in WIPI2-S395A and the reduction in WIPI2-S395D (Figures 4A and 4B). Furthermore, in cells cultured in nutrient-rich medium, the turnover rate of cellular WIPI2-S395A was slower than that of WT WIPI2, while WIPI2-S395D was faster (Figures 4C and 4D). Accordingly, the ubiquitination and HUWE1 binding levels of exogenous WIPI2 were greatly suppressed in WIPI2-S395A-expressing cells and promoted in WIPI2-S395D-expressing cells (Figures 4E–4G and S5A). Notably, treatment with MG132 also accumulated phospho-WIPI2 in MEFs (Figures 4H and 4I). To further verify the link between mTORC1-mediated phosphorylation and HUWE1-dependent ubiquitination of WIPI2, we examined *in vitro* the effect of the phosphorylation of WIPI2 on WIPI2-HUWE1 binding and WIPI2 ubiquitination. Recombinant GST-tagged WIPI2 or WIPI2 mutants were pre-incubated with or without recombinant mTORC1 in the presence of ATP. After being precipitated from the reaction by glutathione Sepharose beads, GST-WIPI2 was incubated with purified recombinant His-HUWE1 with or without purified UBA1, UBCH7, and ubiquitin. Then, the GST-WIPI2 bound His-HUWE1 and the ubiquitination of WIPI2 were checked by western blot using anti-His and anti-ubiquitin, respectively. Clearly, while WIPI2-S395D exhibited higher affinity to HUWE1 and ubiquitination than WT WIPI2 or WIPI2-S395A, which were unchanged by mTORC1 incubation, incubation with mTORC1 significantly enhanced HUWE1 binding and ubiquitination of WT WIPI2, but not of WIPI2-S395A (Figures S5B–S5D). Because PI3P binding and Atg16L1 interaction are characteristic features of WIPI2 and are required for WIPI2 to function in autophagy (Dooley et al., 2014; Polson et al., 2010), we examined the effect of WIPI2 phosphorylation on its affinity for PI3P and Atg16L1. Lipid-protein overlay assay using purified GST-WIPI2s indicated that WIPI2-S395A and WIPI2-S395D exhibited similar affinity to PI3P or PI5P as WT WIPI2 (Polson et al., 2010; Vicinanza et al., 2015) (Figures 4J and 4K). Unexpectedly and intriguingly, GST-WIPI2s showed the strongest binding with PI4P (Figure 4J). In line with this, the colocalization with GFP-tagged DFCP1, a protein that specifically associates with the autophagic pool of PI3P, was not affected by the mutations (Figure 4L). In addition, when purified GST-tagged WT WIPI2 or the WIPI2 mutants were incubated with cell lysates, then precipitated with glutathione Sepharose beads, similar levels of Atg16L1 were pulled down (Figure 4M). Collectively, these data provide evidence that mTORC1-mediated phosphorylation promotes WIPI2 degradation by specifically enhancing the WIPI2-HUWE1 interaction.

mTORC1-Mediated Phosphorylation of WIPI2 Controls Autophagy Intensity

To assess the cell-biological effect of mTORC1-mediated phosphorylation and HUWE1-dependent WIPI2 degradation, we examined their functions in autophagy regulation. We first tested the potential influence of intracellular WIPI2 level on basal autophagy. Under nutrient-rich conditions, overexpression of WIPI2, but not WIPI1, in cells stably expressing GFP-LC3 significantly stimulated the formation of GFP-LC3 puncta (Figures 5A and 5C). Silencing HUWE1 in the cells gave the same results (Figures 5B and 5C). Overexpression of WIPI2 or knockdown of HUWE1 also dramatically promoted the degradation of autophagy receptors p62 and NBR1 (Figures 5D and S6A), which were fully blocked by CQ treatment (Figures 5D and S6A). Furthermore, the degradation of p62 and NBR1 was dose-dependently promoted or inhibited by overexpressing WIPI2 or HUWE1 (Figures S6B–S6E). These results strongly suggest that raising intracellular WIPI2 can elevate basal autophagy. To determine the role of WIPI2 phosphorylation in basal autophagy regulation, we generated GFP-LC3 cells stably expressing WT WIPI2, WIPI2-S395A, or WIPI2-S395D. In fed cells, WIPI2-S395A, but not WIPI2-S395D, further stimulated the formation of GFP-LC3

(F and G) Co-immunoprecipitation of Myc-tagged WIPI2s with transfected His-HUWE1 in the stable cell lines. His-HUWE1 was immunoprecipitated using anti-His. Western blot is presented in (F) and quantification is presented in (G).

(H and I) Phospho-WIPI2 (Ser395) in MEFs treated with MG132. Western blot is presented in (H) and quantification is presented in (I).

(J and K) Purified recombinant GST-tagged WIPI2 or WIPI2 mutants were incubated with PIP strips. Phospholipid-bound WIPI2 was detected with anti-GST (J). Quantification is presented in (K).

(L) Localization of GFP-DFCP1 and Myc-tagged WIPI2 or WIPI2 mutants in MEFs treated with Torin1 for 1 hr. Scale bars, 5 μm.

(M) Purified GST-tagged WIPI1, WIPI2, or WIPI2 mutants were incubated with MEF lysates, and the bound Atg16L1 was detected by western blot. All the statistical data are presented as mean ± SEM of three independent experiments. $^{**}p < 0.01$; $^{***}p < 0.001$.

See also Figure S5.

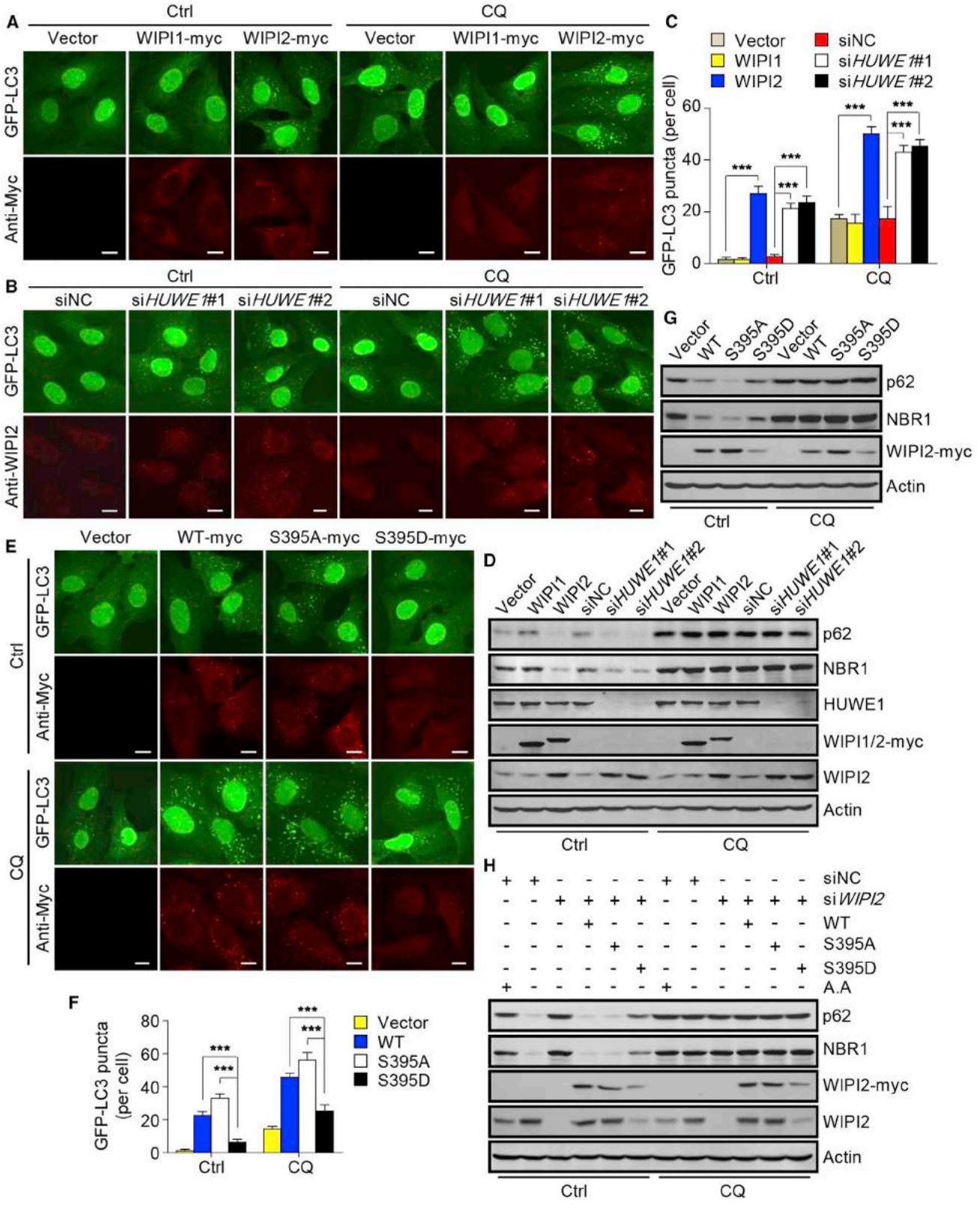

(legend on next page)

puncta and the degradation of p62 and NBR1, compared to WT WIPI2 (Figures 5E–5G and S6F). We also examined the effect of WIPI2 phosphorylation on amino-acid-starvation-induced autophagy. Consistent with previous studies (Polson et al., 2010; Zhao et al., 2017), knocking down WIPI2 in cells suppressed the degradation of p62 and NBR1 when amino acids were removed from the culture medium (Figures 5H and S6G). Re-expression of WT WIPI2 or WIPI2-S395A, but not WIPI2-S395D, in the cells relieved the suppression effects (Figures 5H and S6G). Taken together, these results suggest that mTORC1-mediated WIPI2 phosphorylation is a determinant of basal and induced autophagy controlled by mTORC1.

mTORC1-Mediated Phosphorylation of WIPI2 Regulates Autophagy and Lipid Clearance in Mouse Liver

We then evaluated the physiological function of this mTORC1-WIPI2 pathway in mice. First, we detected a dramatic increase in WIPI2 protein and a decrease in WIPI2 phosphorylation at Ser395 in liver, kidney, and heart tissues of mice that had fasted for 12 hr or 24 hr (Figures 6A and S7), supporting our observations in cells. To obtain direct evidence that WIPI2 phosphorylation regulates liver autophagy in mice, fed mice were intraperitoneally injected with recombinant adeno-associated virus (rAAV) expressing WT WIPI2 (rAAV-WIPI2), WIPI2-S395A (rAAV-WIPI2-S395A), or WIPI2-S395D (rAAV-WIPI2-S395D). Four weeks after the viral infection, no significant difference in body weight of the mice was detected among the groups. In the livers of treated mice, we detected a high level of WIPI2-S395A and a low level of WIPI2-S395D (Figure 6B), reflecting the phosphorylation-based stabilities of the proteins. Nevertheless, compared to WT WIPI2, introduction of WIPI2-S395A, but not WIPI2-S395D, evidently decreased the protein level of p62 and NBR1 in the livers (Figure 6B). In addition, the formation of LC3 puncta (Figures 6C and 6D), the protein level of WIPI2 (Figure 6E), and the degradation of p62 and NBR1 (Figure 6E) were greatly increased in mouse livers injected with rAAV-sh*HUWE1*. Furthermore, we evaluated the function of mTORC1-mediated WIPI2 phosphorylation in lipid clearance in mouse livers, a process that could be mediated by autophagy (Singh et al., 2009). Using oil red O staining of neutral lipids, we found that injection of rAAV-WIPI2 and rAAV-WIPI2-S395A, but not rAAV-WIPI2-S395D, reduced liver neutral lipids and that rAAV-WIPI2-S395A showed a stronger effect than rAAV-WIPI2 (Figures 6F and 6G). These results, therefore, support a physiological function of mTORC1-mediated phosphorylation and the consequent WIPI2 degradation in the regulation of autophagy and autophagy-related lipid clearance in mice.

DISCUSSION

In this study, we have identified that WIPI2 is a novel phosphorylation substrate of mTORC1 and an ubiquitination substrate of HUWE1. By clarifying the link between mTORC1-mediated phosphorylation and HUWE1-dependent ubiquitination of WIPI2, our results suggest a pivotal role of mTORC1 in the post-translational regulation of cellular WIPI2 level, by which mTORC1 precisely controls the intensity of basal autophagy and induced autophagy (Figure 7).

Identification of the effect on WIPI2 pinpoints a surveillance function of mTORC1 in the growth and elongation of autophagic membranes, in addition to its known action in autophagy initiation, nucleation, autophagosome-lysosome fusion, and autophagy termination (Kim et al., 2011; Kim et al., 2015; Yu et al., 2010; Yuan et al., 2013). These findings suggest that mTORC1 is directly involved in the control of all the stages of autophagy, thereby further highlighting mTORC1 as a master switch in autophagy regulation. The participation of mTORC1 in each of the phases enables the coordination of the whole pathway in response to changes in mTORC1 activity so that autophagy can be quickly started and stopped. This mechanism may explain the rapid induction and termination of the complex membrane events of the autophagy process, which allow cells to cope with dynamic changes in the intracellular and extracellular environment.

Our results demonstrate that solely increasing WIPI2 in cells can effectively promote autophagosome formation and autophagic degradation. Under basal cell conditions, WIPI2 is usually expressed at low levels due to the high mTORC1 activity, while it exists in a stable dephosphorylated form when mTORC1 is inactivated during autophagy induction. Our data indicate that WIPI2 expression is related to autophagy intensity, which, in turn, suggests that the intracellular WIPI2 protein level may be a "volume knob" for basal autophagy. The intriguing thing is that phosphorylation of WIPI2 affects its interaction with the E3 ubiquitin ligase HUWE1 for degradation without influencing its affinity for PI3P and Atg16L1 (Dooley et al., 2014; Polson et al., 2010). Because multiple identified HUWE1-binding proteins contain the WD40-repeat domains (Thompson et al., 2014), phosphorylation at Ser395 on WIPI2 may selectively disrupt its interaction with HUWE1, potentially mediated by the WD40-repeat domain, while it interacts with

Figure 5. mTORC1-Mediated Phosphorylation of WIPI2 Controls Autophagy Intensity

(A and B) GFP-LC3 punctum formation in HEK293 cells stably expressing GFP-LC3 with or without CQ treatment for 1 hr. The cells were transfected with WIPI1-myc or WIPI2-myc (A) or incubated with HUWE1 siRNAs (B).

(C) Statistical analysis of the number of GFP-LC3 puncta per cell in (A) and (B).

(D) Degradation of p62 and NBR1 in HEK293 cells treated as in (A) and (B), except that CQ was used for 4 hr.

(E and F) Formation of GFP-LC3 puncta in HEK293 cells stably expressing GFP-LC3 with Myc-tagged WIPI2 or WIPI2 mutants (E). CQ was used for 1 hr. Quantification is presented in (F).

(G) Degradation of p62 and NBR1 in HEK293 cells treated as in (E), except that CQ was used for 4 hr.

(H) Degradation of p62 and NBR1 in amino-acid-deprived HEK293 cells. The cells were transfected with siRNA-resistant, Myc-tagged WIPI2 or WIPI2 mutants 48 hr after WIPI2 RNAi. Amino-acid starvation was carried out 16 hr after transfection with or without CQ for 4 hr.

The data are shown as mean ± SEM; n = 30. ***$p < 0.001$. Scale bars, 10 μm.

See also Figure S6.

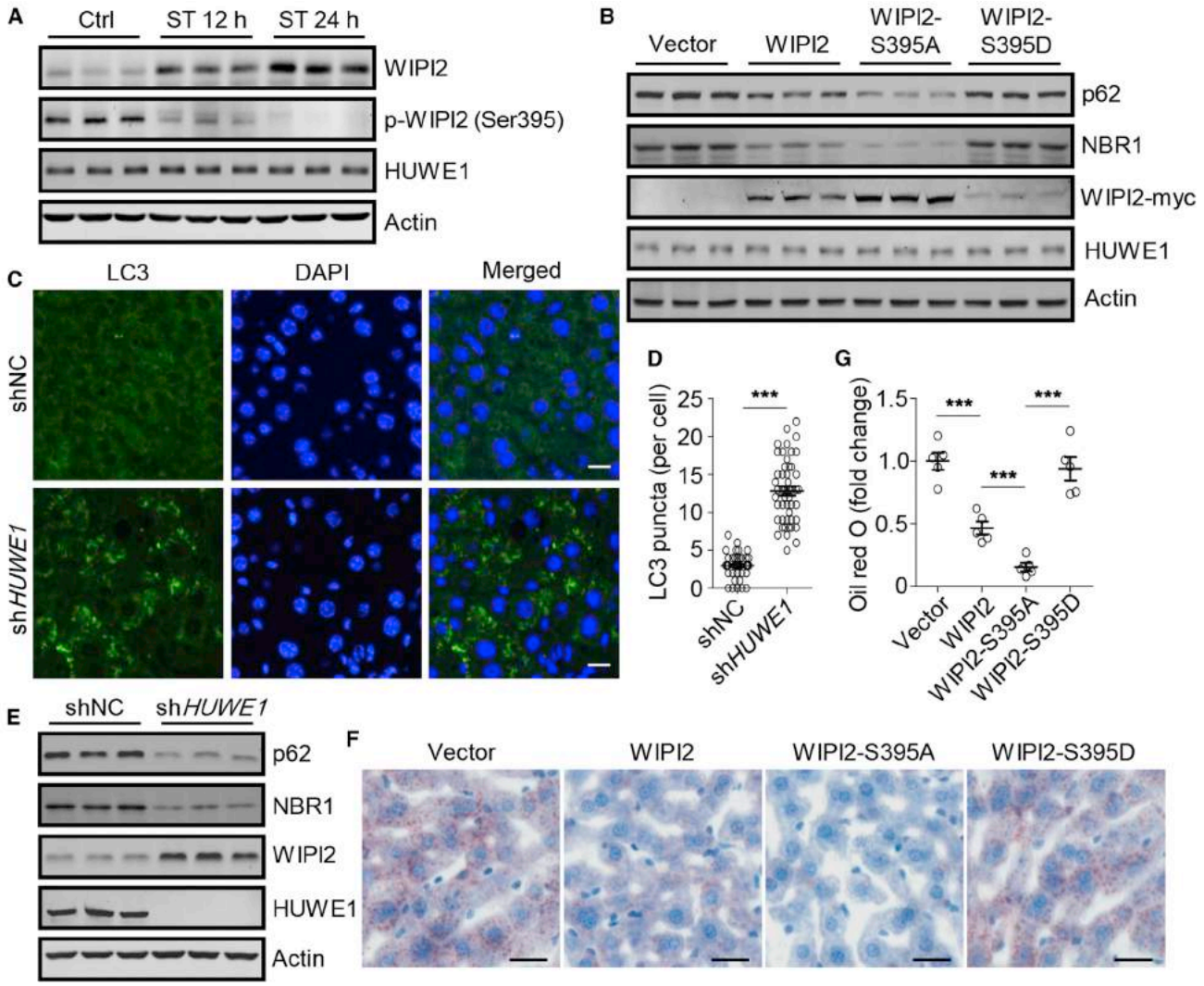

Figure 6. mTORC1-Mediated Phosphorylation of WIPI2 Regulates Autophagy and Lipid Clearance in Mouse Liver

(A) The protein levels of WIPI2 and phospho-WIPI2 (Ser395) in mouse liver tissues. The mice were subjected to starvation for 12 hr or 24 hr.

(B) The protein levels of p62 and NBR1 in mouse liver tissues. The mice were intraperitoneally injected with Myc-tagged rAAV-WT WIPI2, rAAV-WIPI2-S395A, or rAAV-WIPI2-S395D.

(C) Representative LC3 immunostaining in mouse liver tissues. The mice were intraperitoneally injected with rAAV-shNC or rAAV-sh*HUWE1*. Scale bars, 20 μm.

(D) Statistical analysis of the number of LC3 puncta per cell treated as in (C). The data are shown as mean ± SEM; n = 50 from 5 mice. ***$p < 0.001$.

(E) The protein levels of p62 and NBR1 in mouse liver tissues treated as in (C).

(F) Oil red O staining of the mouse liver tissues treated as in (B). Scale bars, 40 μm.

(G) Quantification of intracellular oil red O content in mouse liver tissues treated as in (F). The results are presented as mean ± SEM, n = 5 mice. ***$p < 0.001$. See also Figure S7.

PI3P through its FRRG motif (Baskaran et al., 2012). It is noteworthy that human WIPI2a also can be stabilized by cell starvation, and only WIPI2b is known to be required for autophagy activation (Dooley et al., 2014). Thus, the function of mTORC1-dependent phosphorylation of WIPI2 may not be restricted to the regulation of autophagy. The potential WIPI2 interacting partners identified by our screen, including those involved in membrane trafficking, imply a potential function of WIPI2 and its phosphorylation in other cellular processes. Also, it will certainly be interesting to check whether cells with elevated basal autophagy, such as highly metabolizing cells, express more WIPI2. Specifically, cancer cells, which have a high rate of anabolism and catabolism, as well as elevated mTORC1 activity in most cases (Guertin and Sabatini, 2007), may have an mTORC1-independent mechanism for the regulation of autophagy, including WIPI2 quantity control.

Our *in vitro* lipid-protein overlay assay revealed an unexpected strong affinity of WIPI2 for PI4P. Although it needs to be confirmed in cell, this suggests that WIPI2 could mediate PI4P function on membranes. Considering that *in situ* PI4P

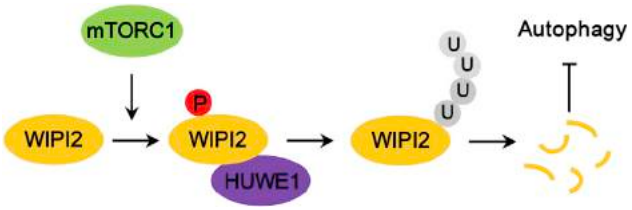

Figure 7. Schematic Model for mTORC1-Regulated and HUWE1-Mediated WIPI2 Degradation in Autophagy

mTORC1 phosphorylates WIPI2 at Ser395. This phosphorylation promotes the binding of WIPI2 with HUWE1, leading to WIPI2 ubiquitination and proteasomal degradation and, thereby, the suppression of autophagy.

production on autophagosomal membranes by GABARAP-mediated recruitment of PI4KIIα has been identified (Wang et al., 2015), and this autophagosome-located PI4P facilitates the fusion of autophagosome with lysosome (Wang et al., 2015), we would propose that WIPI2 on autophagosomes may have a function in autolysosome formation by serving as a PI4P effector.

The identification of HUWE1 as a specific E3 ubiquitin ligase of WIPI2 helps to elucidate not only the molecular mechanism of WIPI2 degradation but also the function of HUWE1 in autophagy regulation. This function of HUWE1 may contribute to its role in autophagy-related cell physiological and pathological processes (Adhikary et al., 2005; Confalonieri et al., 2009).

STAR★METHODS

Detailed methods are provided in the online version of this paper and include the following:

- KEY RESOURCES TABLE
- CONTACT FOR REAGENT AND RESOURCE SHARING
- EXPERIMENTAL MODEL AND SUBJECT DETAILS
  - Cell Culture and Transfection
  - Stable Cell Lines Construction
- METHOD DETAILS
  - Reagents and Treatment
  - Cell Imaging
  - Immunoprecipitation and Western Blot
  - Protein Expression and Purification
  - *In Vitro* Kinase Assay and *In Vitro* Ubiquitination Assay
  - *In Vitro* Pull-Down Assay
  - Lipid-Protein Overlay Assay
  - Lysosomes Isolation
  - Oil Red O Staining
  - RNA Extraction and Real-Time PCR
  - HPLC-MS/MS
  - Mouse Experiments and Tissue Processing
- QUANTIFICATION AND STATISTICAL ANALYSIS
- DATA AND SOFTWARE AVAILABILITY

SUPPLEMENTAL INFORMATION

Supplemental Information includes seven figures and one table and can be found with this article online at https://doi.org/10.1016/j.molcel.2018.09.017.

ACKNOWLEDGMENTS

We are grateful to the Imaging Center of Zhejiang University School of Medicine for their assistance in confocal microscopy. We thank Qiming Sun, Genze Shao, Zongping Xia, Hong Zhang, and Qing Zhong for the sharing of plasmids and reagents. This study was supported by the National Natural Science Foundation of China (31790402, 31530040, and 31671434) and the National Basic Research Program of China (2017YFA0503402).

AUTHOR CONTRIBUTIONS

W.L. and W.W. designed the experiments. W.W., Z.Y., L.Z., and Y.X. performed the experiments. C.P. performed the mass spectrometry. W.L. and W.W. wrote the manuscript. All authors discussed the results and commented on the manuscript.

DECLARATION OF INTERESTS

The authors declare no competing interests.

Received: March 22, 2018
Revised: July 12, 2018
Accepted: September 13, 2018
Published: October 18, 2018

REFERENCES

Abu-Remaileh, M., Wyant, G.A., Kim, C., Laqtom, N.N., Abbasi, M., Chan, S.H., Freinkman, E., and Sabatini, D.M. (2017). Lysosomal metabolomics reveals V-ATPase- and mTOR-dependent regulation of amino acid efflux from lysosomes. Science *358*, 807–813.

Adhikary, S., Marinoni, F., Hock, A., Hulleman, E., Popov, N., Beier, R., Bernard, S., Quarto, M., Capra, M., Goettig, S., et al. (2005). The ubiquitin ligase HectH9 regulates transcriptional activation by Myc and is essential for tumor cell proliferation. Cell *123*, 409–421.

Backer, J.M. (2008). The regulation and function of class III PI3Ks: novel roles for Vps34. Biochem. J. *410*, 1–17.

Baskaran, S., Ragusa, M.J., Boura, E., and Hurley, J.H. (2012). Two-site recognition of phosphatidylinositol 3-phosphate by PROPPINs in autophagy. Mol. Cell *47*, 339–348.

Chang, Y.Y., and Neufeld, T.P. (2009). An Atg1/Atg13 complex with multiple roles in TOR-mediated autophagy regulation. Mol. Biol. Cell *20*, 2004–2014.

Chauhan, S., Goodwin, J.G., Chauhan, S., Manyam, G., Wang, J., Kamat, A.M., and Boyd, D.D. (2013). ZKSCAN3 is a master transcriptional repressor of autophagy. Mol. Cell *50*, 16–28.

Chu, B.B., Liao, Y.C., Qi, W., Xie, C., Du, X., Wang, J., Yang, H., Miao, H.H., Li, B.L., and Song, B.L. (2015). Cholesterol transport through lysosome-peroxisome membrane contacts. Cell *161*, 291–306.

Confalonieri, S., Quarto, M., Goisis, G., Nuciforo, P., Donzelli, M., Jodice, G., Pelosi, G., Viale, G., Pece, S., and Di Fiore, P.P. (2009). Alterations of ubiquitin ligases in human cancer and their association with the natural history of the tumor. Oncogene *28*, 2959–2968.

Dooley, H.C., Razi, M., Polson, H.E., Girardin, S.E., Wilson, M.I., and Tooze, S.A. (2014). WIPI2 links LC3 conjugation with PI3P, autophagosome formation, and pathogen clearance by recruiting Atg12-5-16L1. Mol. Cell *55*, 238–252.

Dunlop, E.A., and Tee, A.R. (2014). mTOR and autophagy: a dynamic relationship governed by nutrients and energy. Semin. Cell Dev. Biol. *36*, 121–129.

Ganley, I.G., Lam, D.H., Wang, J., Ding, X., Chen, S., and Jiang, X. (2009). ULK1.ATG13.FIP200 complex mediates mTOR signaling and is essential for autophagy. J. Biol. Chem. *284*, 12297–12305.

Guertin, D.A., and Sabatini, D.M. (2007). Defining the role of mTOR in cancer. Cancer Cell *12*, 9–22.

Hosokawa, N., Hara, T., Kaizuka, T., Kishi, C., Takamura, A., Miura, Y., Iemura, S., Natsume, T., Takehana, K., Yamada, N., et al. (2009). Nutrient-dependent

mTORC1 association with the ULK1-Atg13-FIP200 complex required for autophagy. Mol. Biol. Cell *20*, 1981–1991.

Hsu, P.P., Kang, S.A., Rameseder, J., Zhang, Y., Ottina, K.A., Lim, D., Peterson, T.R., Choi, Y., Gray, N.S., Yaffe, M.B., et al. (2011). The mTOR-regulated phosphoproteome reveals a mechanism of mTORC1-mediated inhibition of growth factor signaling. Science *332*, 1317–1322.

Huang, R., Xu, Y., Wan, W., Shou, X., Qian, J., You, Z., Liu, B., Chang, C., Zhou, T., Lippincott-Schwartz, J., and Liu, W. (2015). Deacetylation of nuclear LC3 drives autophagy initiation under starvation. Mol. Cell *57*, 456–466.

Itakura, E., and Mizushima, N. (2010). Characterization of autophagosome formation site by a hierarchical analysis of mammalian Atg proteins. Autophagy *6*, 764–776.

Jung, C.H., Jun, C.B., Ro, S.H., Kim, Y.M., Otto, N.M., Cao, J., Kundu, M., and Kim, D.H. (2009). ULK-Atg13-FIP200 complexes mediate mTOR signaling to the autophagy machinery. Mol. Biol. Cell *20*, 1992–2003.

Kim, J., Kundu, M., Viollet, B., and Guan, K.L. (2011). AMPK and mTOR regulate autophagy through direct phosphorylation of Ulk1. Nat. Cell Biol. *13*, 132–141.

Kim, Y.M., Jung, C.H., Seo, M., Kim, E.K., Park, J.M., Bae, S.S., and Kim, D.H. (2015). mTORC1 phosphorylates UVRAG to negatively regulate autophagosome and endosome maturation. Mol. Cell *57*, 207–218.

Lamb, C.A., Yoshimori, T., and Tooze, S.A. (2013). The autophagosome: origins unknown, biogenesis complex. Nat. Rev. Mol. Cell Biol. *14*, 759–774.

Lee, I.H., and Finkel, T. (2009). Regulation of autophagy by the p300 acetyltransferase. J. Biol. Chem. *284*, 6322–6328.

Lee, I.H., Cao, L., Mostoslavsky, R., Lombard, D.B., Liu, J., Bruns, N.E., Tsokos, M., Alt, F.W., and Finkel, T. (2008). A role for the NAD-dependent deacetylase Sirt1 in the regulation of autophagy. Proc. Natl. Acad. Sci. USA *105*, 3374–3379.

Levine, B., and Kroemer, G. (2008). Autophagy in the pathogenesis of disease. Cell *132*, 27–42.

Liu, C.C., Lin, Y.C., Chen, Y.H., Chen, C.M., Pang, L.Y., Chen, H.A., Wu, P.R., Lin, M.Y., Jiang, S.T., Tsai, T.F., and Chen, R.H. (2016). Cul3-KLHL20 ubiquitin ligase governs the turnover of ULK1 and VPS34 complexes to control autophagy termination. Mol. Cell *61*, 84–97.

Martina, J.A., and Puertollano, R. (2013). Rag GTPases mediate amino acid-dependent recruitment of TFEB and MITF to lysosomes. J. Cell Biol. *200*, 475–491.

Mizushima, N., Levine, B., Cuervo, A.M., and Klionsky, D.J. (2008). Autophagy fights disease through cellular self-digestion. Nature *451*, 1069–1075.

Munson, M.J., Allen, G.F., Toth, R., Campbell, D.G., Lucocq, J.M., and Ganley, I.G. (2015). mTOR activates the VPS34-UVRAG complex to regulate autolysosomal tubulation and cell survival. EMBO J. *34*, 2272–2290.

Nojima, H., Tokunaga, C., Eguchi, S., Oshiro, N., Hidayat, S., Yoshino, K., Hara, K., Tanaka, N., Avruch, J., and Yonezawa, K. (2003). The mammalian target of rapamycin (mTOR) partner, raptor, binds the mTOR substrates p70 S6 kinase and 4E-BP1 through their TOR signaling (TOS) motif. J. Biol. Chem. *278*, 15461–15464.

Platta, H.W., Abrahamsen, H., Thoresen, S.B., and Stenmark, H. (2012). Nedd4-dependent lysine-11-linked polyubiquitination of the tumour suppressor Beclin 1. Biochem. J. *441*, 399–406.

Polson, H.E., de Lartigue, J., Rigden, D.J., Reedijk, M., Urbé, S., Clague, M.J., and Tooze, S.A. (2010). Mammalian Atg18 (WIPI2) localizes to omegasome-anchored phagophores and positively regulates LC3 lipidation. Autophagy *6*, 506–522.

Rappsilber, J., Ishihama, Y., and Mann, M. (2003). Stop and go extraction tips for matrix-assisted laser desorption/ionization, nanoelectrospray, and LC/MS sample pretreatment in proteomics. Anal. Chem. *75*, 663–670.

Roczniak-Ferguson, A., Petit, C.S., Froehlich, F., Qian, S., Ky, J., Angarola, B., Walther, T.C., and Ferguson, S.M. (2012). The transcription factor TFEB links mTORC1 signaling to transcriptional control of lysosome homeostasis. Sci. Signal. *5*, ra42.

Sancak, Y., Bar-Peled, L., Zoncu, R., Markhard, A.L., Nada, S., and Sabatini, D.M. (2010). Ragulator-Rag complex targets mTORC1 to the lysosomal surface and is necessary for its activation by amino acids. Cell *141*, 290–303.

Settembre, C., Di Malta, C., Polito, V.A., Garcia Arencibia, M., Vetrini, F., Erdin, S., Erdin, S.U., Huynh, T., Medina, D., Colella, P., et al. (2011). TFEB links autophagy to lysosomal biogenesis. Science *332*, 1429–1433.

Settembre, C., Zoncu, R., Medina, D.L., Vetrini, F., Erdin, S., Erdin, S., Huynh, T., Ferron, M., Karsenty, G., Vellard, M.C., et al. (2012). A lysosome-to-nucleus signalling mechanism senses and regulates the lysosome via mTOR and TFEB. EMBO J. *31*, 1095–1108.

Simonsen, A., and Tooze, S.A. (2009). Coordination of membrane events during autophagy by multiple class III PI3-kinase complexes. J. Cell Biol. *186*, 773–782.

Singh, R., Kaushik, S., Wang, Y., Xiang, Y., Novak, I., Komatsu, M., Tanaka, K., Cuervo, A.M., and Czaja, M.J. (2009). Autophagy regulates lipid metabolism. Nature *458*, 1131–1135.

Suzuki, K., Kubota, Y., Sekito, T., and Ohsumi, Y. (2007). Hierarchy of Atg proteins in pre-autophagosomal structure organization. Genes Cells *12*, 209–218.

Thompson, J.W., Nagel, J., Hoving, S., Gerrits, B., Bauer, A., Thomas, J.R., Kirschner, M.W., Schirle, M., and Luchansky, S.J. (2014). Quantitative Lys-ε-Gly-Gly (diGly) proteomics coupled with inducible RNAi reveals ubiquitin-mediated proteolysis of DNA damage-inducible transcript 4 (DDIT4) by the E3 ligase HUWE1. J. Biol. Chem. *289*, 28942–28955.

Thurston, T.L., Boyle, K.B., Allen, M., Ravenhill, B.J., Karpiyevich, M., Bloor, S., Kaul, A., Noad, J., Foeglein, A., Matthews, S.A., et al. (2016). Recruitment of TBK1 to cytosol-invading *Salmonella* induces WIPI2-dependent antibacterial autophagy. EMBO J. *35*, 1779–1792.

Vicinanza, M., Korolchuk, V.I., Ashkenazi, A., Puri, C., Menzies, F.M., Clarke, J.H., and Rubinsztein, D.C. (2015). PI(5)P regulates autophagosome biogenesis. Mol. Cell *57*, 219–234.

Wan, W., You, Z., Xu, Y., Zhou, L., Guan, Z., Peng, C., Wong, C.C.L., Su, H., Zhou, T., Xia, H., et al. (2017). mTORC1 phosphorylates acetyltransferase p300 to regulate autophagy and lipogenesis. Mol. Cell *68*, 323–335.e6.

Wang, H., Sun, H.Q., Zhu, X., Zhang, L., Albanesi, J., Levine, B., and Yin, H. (2015). GABARAPs regulate PI4P-dependent autophagosome:lysosome fusion. Proc. Natl. Acad. Sci. USA *112*, 7015–7020.

Wei, Y., Zou, Z., Becker, N., Anderson, M., Sumpter, R., Xiao, G., Kinch, L., Koduru, P., Christudass, C.S., Veltri, R.W., et al. (2013). EGFR-mediated Beclin 1 phosphorylation in autophagy suppression, tumor progression, and tumor chemoresistance. Cell *154*, 1269–1284.

Wirth, M., Joachim, J., and Tooze, S.A. (2013). Autophagosome formation–the role of ULK1 and Beclin1-PI3KC3 complexes in setting the stage. Semin. Cancer Biol. *23*, 301–309.

Xu, Y., Wan, W., Shou, X., Huang, R., You, Z., Shou, Y., Wang, L., Zhou, T., and Liu, W. (2016). TP53INP2/DOR, a mediator of cell autophagy, promotes rDNA transcription via facilitating the assembly of the POLR1/RNA polymerase I pre-initiation complex at rDNA promoters. Autophagy *12*, 1118–1128.

Yang, Z., and Klionsky, D.J. (2010). Mammalian autophagy: core molecular machinery and signaling regulation. Curr. Opin. Cell Biol. *22*, 124–131.

Yang, G., Li, Q., Ren, S., Lu, X., Fang, L., Zhou, W., Zhang, F., Xu, F., Zhang, Z., Zeng, R., et al. (2009). Proteomic, functional and motif-based analysis of C-terminal Src kinase-interacting proteins. Proteomics *9*, 4944–4961.

Yang, Y., Do, H., Tian, X., Zhang, C., Liu, X., Dada, L.A., Sznajder, J.I., and Liu, J. (2010). E3 ubiquitin ligase Mule ubiquitinates Miz1 and is required for TNFalpha-induced JNK activation. Proc. Natl. Acad. Sci. USA *107*, 13444–13449.

Yang, Y., Fiskus, W., Yong, B., Atadja, P., Takahashi, Y., Pandita, T.K., Wang, H.G., and Bhalla, K.N. (2013). Acetylated hsp70 and KAP1-mediated Vps34 SUMOylation is required for autophagosome creation in autophagy. Proc. Natl. Acad. Sci. USA *110*, 6841–6846.

Yu, L., McPhee, C.K., Zheng, L., Mardones, G.A., Rong, Y., Peng, J., Mi, N., Zhao, Y., Liu, Z., Wan, F., et al. (2010). Termination of autophagy and reformation of lysosomes regulated by mTOR. Nature *465*, 942–946.

Yu, Y., Yoon, S.O., Poulogiannis, G., Yang, Q., Ma, X.M., Villén, J., Kubica, N., Hoffman, G.R., Cantley, L.C., Gygi, S.P., and Blenis, J. (2011). Phosphoproteomic analysis identifies Grb10 as an mTORC1 substrate that negatively regulates insulin signaling. Science *332*, 1322–1326.

Yu, L., Chen, Y., and Tooze, S.A. (2018). Autophagy pathway: Cellular and molecular mechanisms. Autophagy *14*, 207–215.

Yuan, H.X., Russell, R.C., and Guan, K.L. (2013). Regulation of PIK3C3/VPS34 complexes by MTOR in nutrient stress-induced autophagy. Autophagy *9*, 1983–1995.

Zhang, J., Kan, S., Huang, B., Hao, Z., Mak, T.W., and Zhong, Q. (2011). Mule determines the apoptotic response to HDAC inhibitors by targeted ubiquitination and destruction of HDAC2. Genes Dev. *25*, 2610–2618.

Zhang, T., Dong, K., Liang, W., Xu, D., Xia, H., Geng, J., Najafov, A., Liu, M., Li, Y., Han, X., et al. (2015). G-protein-coupled receptors regulate autophagy by ZBTB16-mediated ubiquitination and proteasomal degradation of Atg14L. eLife *4*, e06734.

Zhao, Y.G., Chen, Y., Miao, G., Zhao, H., Qu, W., Li, D., Wang, Z., Liu, N., Li, L., Chen, S., et al. (2017). The ER-localized transmembrane protein EPG-3/VMP1 regulates SERCA activity to control ER-isolation membrane contacts for autophagosome formation. Mol. Cell *67*, 974–989.e6.

STAR★METHODS

KEY RESOURCES TABLE

REAGENT or RESOURCE	SOURCE	IDENTIFIER
Antibodies		
Rabbit polyclonal anti-GFP	Abcam	Cat#ab290; RRID: AB_303395
Rabbit monoclonal anti-Atg16L1	Abcam	Cat#ab187671
Rabbit monoclonal anti-ULK1	Abcam	Cat#ab128859; RRID: AB_11156928
Mouse monoclonal anti-WIPI2	Abcam	Cat#ab105459; RRID: AB_10860881
Rabbit monoclonal anti-NBR1	Cell Signaling Technology	Cat#9891; RRID: AB_10949888
Rabbit polyclonal anti-S6K1	Cell Signaling Technology	Cat#9202; RRID: AB_331676
Rabbit polyclonal anti-phospho-S6K1 (Thr389)	Cell Signaling Technology	Cat#9205; RRID: AB_330944
Mouse monoclonal anti-HUWE1	Cell Signaling Technology	Cat#5695; RRID: AB_10922588
Rabbit polyclonal anti-WIPI2	Cell Signaling Technology	Cat#8567; RRID: AB_11178945
Rabbit polyclonal anti-phospho-WIPI2 (Ser395 in mouse WIPI2)	Cell Signaling Technology	Cat#13571
Rabbit monoclonal anti-Raptor	Cell Signaling Technology	Cat#2280; RRID: AB_561245
Mouse monoclonal anti-LC3	Cosmo Bio	Cat#CAC-CTB-LC3-2-IC; RRID: AB_10707197
Rabbit polyclonal anti-Atg5	Novus Biologicals	Cat#NB110-53818; RRID: AB_828587
Rabbit polyclonal anti-p62/SQSTM1	Proteintech	Cat#18420-1-AP; RRID: AB_10694431
Rabbit polyclonal anti-Beclin 1	Proteintech	Cat#11306-1-AP; RRID: AB_2259061
Mouse monoclonal anti-GFP	Santa Cruz Biotechnology	Cat#sc-9996; RRID: AB_627695
Mouse monoclonal anti-Myc	Santa Cruz Biotechnology	Cat#sc-40; RRID: AB_627268
Rabbit polyclonal anti-GST	Santa Cruz Biotechnology	Cat#sc-459; RRID: AB_631586
Mouse monoclonal anti-Flag	Santa Cruz Biotechnology	Cat#sc-51590; RRID: AB_677316
Rabbit polyclonal anti-Flag	Santa Cruz Biotechnology	Cat#sc-807; RRID: AB_675756
Rabbit polyclonal anti-His	Santa Cruz Biotechnology	Cat#sc-803; RRID: AB_631655
Mouse monoclonal anti-Ubiquitin	Santa Cruz Biotechnology	Cat#sc-8017; RRID: AB_628423
Rabbit polyclonal anti-Atg7	Sigma-Aldrich	Cat#A2856; RRID: AB_1078239
Mouse monoclonal anti-β-Actin	Sigma-Aldrich	Cat#A5316; RRID: AB_476743
Mouse monoclonal anti-β-Tubulin	Sigma-Aldrich	Cat#T8328; RRID: AB_1844090
Rabbit polyclonal anti-WIPI2	Sigma-Aldrich	Cat#SAB4200399
Mouse monoclonal anti-phospho-Ser/Thr-Pro	Millipore	Cat#05-368; RRID: AB_309698
Donkey anti-rabbit IgG (H+L) IRDye800CW	LI-COR Biosciences	Cat#926-32213; RRID: AB_621848
Donkey anti-mouse IgG (H+L) IRDye680RD	LI-COR Biosciences	Cat#926-68072; RRID: AB_10953628
Goat anti-Mouse IgG (H+L), Alexa Fluor 488	Thermo Fisher Scientific	Cat#A-11001; RRID: AB_2534069
Donkey anti-Mouse IgG (H+L), Alexa Fluor 546	Thermo Fisher Scientific	Cat#A10036; RRID: AB_2534012
Glutathione-Sepharose 4B beads	GE Healthcare Life Sciences	Cat#17-0756-01
Protein G PLUS-Agarose	Santa Cruz Biotechnology	Cat#sc-2002
Protein A-Agarose	Santa Cruz Biotechnology	Cat#sc-2001
Nickel magnetic agarose beads	Sigma-Aldrich	Cat#H9914
Anti-Myc affinity beads	Biotool	Cat#B23402
Bacterial and Virus Strains		
E. coli BL21	Transgen Biotech	Cat#CD601
E. coli Trans 5α	Transgen Biotech	Cat#CD201
Chemicals, Peptides, and Recombinant Proteins		
Lipofectamine 2000	Invitrogen	Cat#11668019
mTOR assay buffer	Invitrogen	Cat#PV4794
TRIzol reagent	Invitrogen	Cat#15596026

(*Continued on next page*)

Continued

REAGENT or RESOURCE	SOURCE	IDENTIFIER
Protease inhibitor Cocktail tablet	Roche	Cat#04693132001
Phosphatase inhibitor	Sangon Biotech	Cat#C500017
Creatine phosphate	Santa Cruz Biotechnology	Cat#sc-221442
Ubiquitin aldehyde	Santa Cruz Biotechnology	Cat#sc-4316
2-Chloroacetamide	Sigma-Aldrich	Cat#C0267
Chloroquine	Sigma-Aldrich	Cat#C6628
Cycloheximide	Sigma-Aldrich	Cat#C7698
MG132	Sigma-Aldrich	Cat#SML1135
Imidazole	Sigma-Aldrich	Cat#I5513
Recombinant mTORC1	Sigma-Aldrich	Cat#SRP0364
Torin1	Tocris Biosciences	Cat#4247
Critical Commercial Assays		
BCA protein assay kit	Thermo Fisher Scientific	Cat#23227
Deposited Data		
Original images were deposited to Mendeley data	This paper	https://doi.org/10.17632/gm6kwj8xvz.1
Experimental Models: Cell Lines		
HEK293	ATCC	ATCC CRL-1573
HEK293T	Donated by Qiming Sun	N/A
WT immortalized MEFs	Huang et al., 2015	N/A
Atg5$^{-/-}$ immortalized MEFs	Huang et al., 2015	N/A
TSC1$^{-/-}$ immortalized MEFs	Wan et al., 2017	N/A
TSC2$^{-/-}$ immortalized MEFs	Wan et al., 2017	N/A
GFP-LC3 HEK293	Huang et al., 2015	N/A
WIPI2-myc HEK293T	Constructed in our lab	N/A
WIPI2-S395A-myc HEK293T	Constructed in our lab	N/A
WIPI2-S395D-myc HEK293T	Constructed in our lab	N/A
GFP-LC3 HEK293 expressing WIPI2-myc	Constructed in our lab	N/A
GFP-LC3 HEK293 expressing WIPI2-S395A-myc	Constructed in our lab	N/A
GFP-LC3 HEK293 expressing WIPI2-S395D-myc	Constructed in our lab	N/A
Oligonucleotides		
Human HUWE1 siRNA1GAGUUUGGAGUUUGUGAAGUUTT	This paper	N/A
Human HUWE1 siRNA2UGCCGCAAUCCAGACAUAUTT	This paper	N/A
Mouse HUWE1 siRNA1GAAUUUGGAGUAUGUGAAGUUTT	This paper	N/A
Mouse HUWE1 siRNA2UGCCGCAAUCCAGACAUAUTT	This paper	N/A
Human WIPI2 siRNAGACAGUCCUUUAGCGGCATT	This paper	N/A
Non-targeting siRNAUUCUCCGAACGUGUCACGUTT	This paper	N/A
Recombinant DNA		
WIPI2-myc	This paper	N/A
WIPI2-S395A-myc	This paper	N/A
WIPI2-S395D-myc	This paper	N/A
WIPI2-5KR-myc	This paper	N/A
WIPI1-myc	This paper	N/A
GST-WIPI2	This paper	N/A
GST-WIPI2-S395A	This paper	N/A
GST-WIPI2-S395D	This paper	N/A
GST-WIPI1	This paper	N/A
GST-histone H3	Wan et al., 2017	N/A

(*Continued on next page*)

Continued

REAGENT or RESOURCE	SOURCE	IDENTIFIER
TMEM192-GFP	This paper	N/A
GFP-LC3	Huang et al., 2015	N/A
GFP-DFCP1	This paper	N/A
WIPI2a-GFP	This paper	N/A
WIPI2b-GFP	This paper	N/A
WIPI2c-GFP	This paper	N/A
WIPI2d-GFP	This paper	N/A
His-UBCH7-C86A	This paper	N/A
His-HUWE1-C4341A	This paper	N/A
TFEB-Flag	This paper	N/A
His-HUWE1	Donated by Genze Shao	N/A
Flag-ubiquitin	Donated by Tianhua Zhou	N/A
His-ubiquitin	Donated by Zongping Xia	N/A
His-UBA1	Donated by Zongping Xia	N/A
His-UBCH7	Donated by Zongping Xia	N/A
cDNA of mouse WIPI2	Donated by Hong Zhang	N/A
cDNA of mouse WIPI1	Donated by Hong Zhang	N/A
cDNA of human WIPI2a	Donated by Jiahuai Han	N/A
cDNA of human WIPI2b	Donated by Han-Ming Shen	N/A
cDNA of human WIPI2c	Donated by Han-Ming Shen	N/A
cDNA of human WIPI2d	Donated by Han-Ming Shen	N/A
cDNA of human TMEM192	Donated by Jiahuai Han	N/A
Software and Algorithms		
Odyssey infrared imaging system	LI-COR Biosciences	N/A
DNA STAR sequence assay	DNASTAR	http://www.dnastar.com
LSM 510 software	Zeiss	N/A
ABI7500 real-time PCR system	Applied Biosystems	N/A
GraphPad Prism software	GraphPad Software	http://www.graphpad.com
Other		
All restriction enzymes	Thermo Fisher Scientific	N/A
KOD-plus-neo	TOYOBO	Cat#KOD-401
PIP Strips	Echelon	Cat#P-6001

CONTACT FOR REAGENT AND RESOURCE SHARING

Further information and requests for reagents may be directed to, and will be fulfilled by Lead Contact Wei Liu (liuwei666@zju.edu.cn).

EXPERIMENTAL MODEL AND SUBJECT DETAILS

Cell Culture and Transfection

HEK293, HEK293T cells and MEFs were cultured in DMEM supplemented with 10% FBS. Lipofectamine 2000 was used for plasmids transient transfection according to the manufacturer's instructions. Cells were analyzed 16-24 hr after transfection. For RNA interference, siRNA duplexes were transfected twice with an interval of 24 hr to achieve the maximal RNAi efficacy.

Stable Cell Lines Construction

HEK293 cells stably expressing GFP-LC3 were generated as described previously (Huang et al., 2015). GFP-LC3 HEK293 and HEK293T cells stably expressing WIPI2-myc, WIPI2-S395A-myc or WIPI2-S395D-myc were generated by transient transfection followed by selection with puromycin.

METHOD DETAILS

Reagents and Treatment

The chemicals were used as follows unless indicated otherwise: Torin1, 50 nM, 3 hr; chloroquine (CQ), 10 μM, 6 hr; MG132, 5 μM, 6 hr; cycloheximide (CHX), 5 μM. Cells were incubated with EBSS for 3 hr, referred to as starvation, or were cultured in amino acid-free medium containing 10% dialyzed FBS for 4 hr, referred to as amino acid starvation.

Cell Imaging

For immunostaining, HEK293 cells or MEFs were fixed with 4% formaldehyde in PBS for 15 min at room temperature and permeabilized with 0.1% saponin in PBS for 10 min. Then the cells were incubated with appropriate primary and secondary antibodies in 0.1% saponin as indicated. Confocal images were captured in multi-tracking mode on a laser scanning confocal microscope with a 63 × plan apochromat 1.4 NA objective. To quantify the number of GFP-LC3 puncta, a total of 30 cells were recorded and analyzed using the Axiovision Automatic Measurement Program on the Zeiss LSM800. GFP-LC3 puncta with diameters between 0.3 μm and 1 μm were scored as positive.

For LC3 assessment in tissue samples, fresh liver tissues were harvested and immediately frozen in liquid nitrogen. Then the liver tissues were embedded in Tissue-Tek OCT compound and stored at −80°C. The samples were sectioned at 5 mm on a cryostat (CM1950, Leica). Immunostaining of LC3 was performed as described above.

Immunoprecipitation and Western Blot

For immunoprecipitation between mTORC1 and WIPI2, cells were lysed in CHAPS buffer (50 mM HEPES, pH 7.4, 150 mM NaCl, 2 mM EDTA, 1 mM orthovanadate, 50 mM NaF, 10 mM pyrophosphate, and 0.3% CHAPS) supplemented with a complete protease inhibitor cocktail and mixed with antibodies at 4°C for 4 hr, followed by the addition of protein A/G agarose beads. Immunocomplexes were washed extensively 4 times with high-salt CHAPS buffer (0.5 M NaCl) and subjected to western blot. For analysis of WIPI2 ubiquitination, cells were lysed in UREA buffer (50 mM Tris-HCl, pH 8.0, 100 mM NaH_2PO_4, 8 M urea, 40 mM imidazole, and 0.5% CHAPS) supplemented with protease inhibitors. Otherwise, cells were lysed in Nonidet P40 (NP-40) buffer (50 mM Tris-HCl, pH 7.4, 1% NP-40, 150 mM NaCl, 2 mM EDTA, 1mM DTT, 10% glycerol) supplemented with protease inhibitors.

Western blot was performed as described previously (Xu et al., 2016). In brief, samples were separated with SDS-PAGE, transferred to polyvinylidene difluoride membrane and probed with the corresponding antibodies. The specific bands were analyzed using an Odyssey Infrared Imaging System.

Protein Expression and Purification

GST-tagged WIPI1, WIPI2 and WIPI2 mutants, histone H3, and His-tagged ubiquitin, UBA1 (E1), UBCH7 (E2) and UBCH7 inactive mutant were expressed in *Escherichia coli* BL21 by induction with 0.1 mM isopropyl β-D-thiogalactopyranoside for 12 hr at 28°C. His-tagged HUWE1 and HUWE1 inactive mutant were expressed in HEK293T cells. GST-tagged recombinant proteins and His-tagged recombinant proteins were purified using glutathione-Sepharose 4B beads and nickel magnetic agarose beads, respectively, according to the manufacturers' instructions. Then the glycerol was added to a final concentration of 25% into the eluates for storage at −80°C.

In Vitro Kinase Assay and *In Vitro* Ubiquitination Assay

In vitro kinase assay was performed as described previously (Yu et al., 2011). Briefly, purified recombinant GST-WIPI2 was incubated with recombinant mTORC1 in 50 μl reaction mixture at 37°C for 30 min. The reaction mixture contained 1 × mTORC1 kinase buffer, protease inhibitors, 2 mM DTT, 10 μM ATP, 1 μg GST-WIPI2, and 250 ng mTORC1.

In vitro ubiquitination assay was performed in 50 μl reaction mixture at 37°C for 2 hr as described previously with some modifications (Yang et al., 2010; Zhang et al., 2011). The reaction mixture contained 100 ng purified recombinant GST-WIPI2, 100 ng purified recombinant UBA1 (E1), 500 ng UBCH7 (E2), 10 μg ubiquitin and 2.5 μg purified recombinant HUWE1, in an ATP-regenerating system (50 mM Tris-HCl, pH 7.6, 5 mM $MgCl_2$, 2 mM ATP, 10 mM creatine phosphate, 3.5 U/mL creatine kinase, and 0.6 U/mL inorganic pyrophosphatase), in the presence of ubiquitin aldehyde (5 μM) and MG132 (50 μM).

Phosphorylation-ubiquitination coupled assay. After the *in vitro* kinase assay, GST-tagged WIPI2 or WIPI2 mutants were precipitated by glutathione-Sepharose 4B beads and washed with ubiquitination reaction buffer. Then the precipitated GST-WIPI2 was subjected to *in vitro* ubiquitination assay.

All the reactions were terminated by the addition of the SDS sample buffer. The samples were then subjected to western blot.

In Vitro Pull-Down Assay

For protein pull-down assay, purified GST, GST-histone H3, GST-WIPI1, GST-WIPI2 proteins were incubated with recombinant mTORC1, purified recombinant His-HUWE1, or cell lysates for 4 hr at 4°C. Then glutathione-Sepharose 4B beads were added to the mixture, followed by further incubation for 2 hr at 4°C. The beads were washed with Nonidet P40 (NP-40) buffer (50 mM Tris-HCl, pH 7.4, 1% NP-40, 150 mM NaCl, 2 mM EDTA, 1mM DTT, 10% glycerol) for 4 times. The beads-bound materials were subjected to western blot.

Phosphorylation-pull down coupled assay. After the *in vitro* kinase assay, GST-tagged WIPI2 or WIPI2 mutants were precipitated by glutathione-Sepharose 4B beads and washed with NP-40 buffer. Then the precipitated GST-tagged WIPI2 or WIPI2 mutants were subjected to *in vitro* pull-down assay by incubating with purified recombinant His-HUWE1.

Lipid-Protein Overlay Assay

Purified GST-tagged WIPI2, or WIPI2 mutants were used to overlay membrane-immobilized phospholipid membranes. GST-tagged proteins were detected using anti-GST and anti-rabbit secondary antibody and scanned with an Odyssey Infrared Imaging System.

Lysosomes Isolation

Lysosomes were isolated as described previously with some modifications (Abu-Remaileh et al., 2017; Chu et al., 2015). Briefly, MEFs transiently transfected with TMEM192-GFP were harvested, washed, and homogenized in extraction buffer (5 mM MOPS, pH 7.65, 0.25 M sucrose, 1 mM EDTA, 0.1% ethanol, and protease inhibitors). The lysates were incubated with a specific GFP antibody at 4°C for 4 hr, followed by the addition of protein A agarose beads for 2 hr. The bound lysosomes were washed using extraction buffer for 4 times and subjected to western blot.

Oil Red O Staining

Mouse liver tissues were fixed in ice-cold 4% (w/v) paraformaldehyde for 24 hr. Liver sections were washed twice with PBS, stained with oil red O solution (Sangon Biotech), differentiated with 50% ethanol, rinsed with tap water and finally counterstained with hematoxylin staining solution (Sangon Biotech).

To quantify oil red O content levels, isopropanol was added to each sample shaken at room temperature for 5 min, and each sample was assessed spectrophotometrically at 510 nm.

RNA Extraction and Real-Time PCR

Total RNA was isolated from cells using Trizol. Reverse transcription was performed using M-MLV reverse transcription reagents (Promega). The resulting cDNA was subjected to real-time PCR analysis with gene-specific primers in the presence of SYBR Green PCR Master Mix (Takara) using the ABI7500 real-time PCR system. The primers used, *WIPI2* forward, ACTGGCTACTTTGGG AAGGTTCT, *WIPI2* reverse, AGATGCAGAGTCTACGAT; *ACTB* forward, AGGGAAATCGTGCGTGACATCAA, *ACTB* reverse, ACCCAAGAAGGAAGGCTGGAAAA.

HPLC-MS/MS

To prepare samples for mass spectrometric analysis of ubiquitination site(s) of WIPI2 by HUWE1, recombinant GST-WIPI2 was incubated with recombinant UBA1 (E1), UBCH7 (E2), ubiquitin, and purified recombinant HUWE1, in an ATP-regenerating system. The samples were blocked with 2-chloroacetamide for 30 min at 30°C before loading to the gel (Yang et al., 2009). The extracts were then desalted and concentrated using StageTip and the eluted peptides were subjected to mass spectrometric analysis (Rappsilber et al., 2003).

To prepare samples for mass spectrometric analysis of phosphorylation site(s) of WIPI2 by mTORC1, recombinant GST-WIPI2 was incubated with recombinant mTORC1 in the presence of ATP, and then separated by SDS-PAGE and depicted with colloidal Coomassie blue staining. Following reduction and alkylation, in-gel digestion of WIPI2 was performed with MS-grade modified trypsin (Promega) at 37°C overnight. The peptides were extracted twice with 1% trifluoroacetic acid in 50% acetonitrile aqueous solution. The extracts were then combined and dried in a Speedvac.

To characterize the interaction proteins of WIPI2, HEK293T cells stably expressing WIPI2-myc were immunoprecipitated with anti-Myc agarose beads. The agarose beads were washed 4 times with Tris-HCl (100 mM, pH 8.5), and then dissolved with 40 μL urea (8 M)/DTT (10 mM). The mixture was sonicated for 30 min at room temperature, and then sequentially treated with IAA (10 mM) and trypsin to alkylate the resulting thiol group and digest the proteins for 16 hr at 37°C at an enzyme-to-substrate ratio of 1:50 (w/w).

For LC-MS/MS analysis, the tryptic digested peptides were directly loaded onto an in-house packed capillary reverse-phase C18 column (150 mm length, 360 μm OD × 75 μm ID, 2.5 μm particle, 100 Å pore diameter) connected to an Agilent HPLC1260 system (Agilent Technology) and then desalted online for 60 min. The samples were analyzed with a 180 min-HPLC gradient from 0% to 100% of 0.1% formic acid in acetonitrile at a flow rate of 300 nl/min. The eluted peptides were ionized and directly introduced into a Q-Exactive mass spectrometer (Thermo Fisher Scientific) using a nano-spray source. Survey full-scan MS spectra (m/z 300–1800) were acquired in the Orbitrap analyzer with resolution r = 70,000 at m/z 400.

Mouse Experiments and Tissue Processing

Male C57BL/6 mice (Seven weeks of age) were housed under a 12 hr light/dark cycle with access to food and water *ad libitum*. For fasting, mice were subjected to 12 hr or 24 hr food starvation. These mice had free access to water. For immunostaining experiments, fresh liver tissues were immediately frozen in liquid nitrogen.

For investigating the role of HUWE1-dependent ubiquitination and mTORC1-mediated phosphorylation of WIPI2 in regulating autophagy *in vivo*, recombinant adeno-associated virus vectors packing non-targeting shRNA (rAAV-shNC) and

HUWE1 shRNA (rAAV-sh*HUWE1*), and recombinant adeno-associated virus vectors packing WT WIPI2 (rAAV-WIPI2), WIPI2-S395A (rAAV-WIPI2-S395A), or WIPI2-S395D (rAAV-WIPI2-S395D) and pseudoserotyped AAV9 caspid (Vigene Biosciences, Shandong, China), were produced in HEK293T cells. Mice were intraperitoneally injected with the viruses. Four weeks after viral injection, the mice were sacrificed for the analysis.

All animal studies and experimental procedures were approved by the Animal Care and Use Committee of the animal facility at Zhejiang University.

QUANTIFICATION AND STATISTICAL ANALYSIS

All the statistical data are presented as mean ± SEM. The statistical significance of differences was determined using Student's t test. $p < 0.05$ was considered to be statistically significant.

DATA AND SOFTWARE AVAILABILITY

Original images were deposited to Mendeley data at https://doi.org/10.17632/gm6kwj8xvz.1.